Journal of Applied Physics ARTICLE scitation.org/journal/jap

Plasma charge injection technology and its application to c-Si solar cells for field-effect passivation

Cite as: J. Appl. Phys. **125**, 173301 (2019); doi: 10.1063/1.5087725
Submitted: 3 January 2019 · Accepted: 2 April 2019 ·
Published Online: 1 May 2019

View Online Export Citation CrossMark

Jeong-Mo Hwang[a)]

AFFILIATIONS

Amtech Systems, Inc. 131 S. Clark Drive, Tempe, Arizona 85281, USA

[a)]jhwang@amtechsystems.com

ABSTRACT

A plasma charge injection technology applicable for field-effect passivation in crystalline silicon solar cells is discussed. The technology uses an inert-gas plasma (helium, argon, N_2, etc.) as a charge source and a DC bias to extract desired charges from a remote plasma source. A charging model is proposed, and it gives a good guideline to determine a proper charging operation condition for a desired injection charge density. The technology can introduce electric charges into a nitride–oxide or oxide–nitride–oxide passivation stack in a few hundred milliseconds with a charge density equivalent to or higher than that of Al_2O_3 in a range of 5×10^{12} to 8×10^{12} cm^{-2}. Most-like charge injection mechanisms are discussed for both negative and positive charging. This technology uses a cheap inert-gas plasma which does not cause any parasitic film deposition nor any corrosion inside the chamber during the charging operation and, thus, does not require regular maintenance for chamber cleaning, which leads to a very low cost of ownership. This charging technology is promising for a low-cost alternative to the complex Al_2O_3 technology. This plasma charge injection can be another important application of the plasma technology among other well-known applications such as dry etching, thin-film deposition, sputtering, etc.

I. INTRODUCTION

Surface passivation becomes more critical to further enhance the solar cell efficiency as the silicon wafer bulk quality gets better and the wafer thickness gets thinner. There are two types of surface passivation:[1] chemical passivation and field-effect passivation. Chemical passivation is to chemically passivate electrically active surface defects such as hydrogen passivation of interface states associated with surface silicon dangling bonds. Field-effect passivation is to suppress the surface recombination by forming a strong surface accumulation layer by fixed charges present in a passivation dielectric film which repels photo-generated minority carriers away from the silicon surface.

SiN_x (silicon-nitride) film deposited by PECVD (Plasma-Enhanced Chemical Vapor Deposition) has been widely used for an anti-reflective coating as well as for a surface passivation in crystalline silicon solar cells.[2,3] PECVD SiN_x film contains positive fixed charges and is good for field-effect passivation to an n-type silicon surface such as n+ emitter in p-type cells or n+ BSF (Back Surface Field) in n-type cells.

On the other hand, positive fixed charges in a PECVD SiN_x film can have detrimental effects on p-type surface passivation, because positive charges attract minority carriers, electrons, in this case, which will be lost at the surface by recombination with majority carriers, which are holes. In the case of lightly doped p-type substrate in PERC (Passivated Emitter and Rear Cell),[4] SiN_x positive fixed charges invert p-type (holes) to n-type (electrons at the surface). In this inversion case, although the surface passivation is as good as that for accumulation by negative charges, cell efficiency is known to be degraded by parasitic shunting.[5]

So, for p-type passivation, industry uses aluminum oxide (Al_2O_3) passivation which contains a high density of negative fixed charges.[6,7] Two typical applications of the Al_2O_3 passivation are p-type rear surface passivation in p-type PERC (Passivated Emitter and Rear Cell)[8,9] and front p+ emitter passivation in n-type PERT (Passivated Emitter and Rear Totally doped) or PERL (Passivated Emitter and Rear Locally diffused) cells.[10]

However, there are two big drawbacks of this Al_2O_3 technology: cost and safety. Its high cost is associated with a high capital

expenditure of the processing equipment and additionally with a high operation expense (OPEX). The high OPEX is due to the use of the precursor material, TMA (tri-methyl-aluminum) and a maintenance cost to clean Al_2O_3 powders in the chamber as well as in exhaust lines. The safety concern is because TMA in gas or liquid form tends to explode when it is exposed to air. A tight control for safety adds an additional cost.

In this work, we introduce negative charges into a SiN_x passivation film, which would replace the complex Al_2O_3 process. In a semiconductor nonvolatile memory known as SONOS (silicon–oxide–nitride–oxide–silicon),[11] it is well known that silicon nitride (SiN_x) stores charges by trapping electrons or holes at bandgap trap centers. Electrons or holes are injected from a silicon substrate by applying a DC bias pulse to the gate electrode on the ONO (oxide/nitride/oxide) gate dielectric stack.

The challenge in solar cells is how to inject charges into a SiN_x dielectric film with no electrode on open passivation areas. Corona Discharge[12] is a well-known method to introduce charges onto an open area of dielectric passivation films. There are reports on the charging of passivation films using this method at a laboratory scale.[13–15] This method uses air ionization with a very high voltage in the range of a few kilovolts or higher. Issues with this method include high-voltage safety, cell damage, electrode corrosion by radical oxygen and/or water molecules, etc.

We invented a plasma charging technology which uses a much lower DC bias around 100 V and an inert-gas plasma which does not cause corrosion or parasitic film deposition inside the chamber, and have two patents granted on this technology (US 8,338,211 B2 in 2012 and US 9,520,531 B2 in 2016). We have successfully demonstrated its applications with flat-band voltage shifts in capacitance–voltage (C–V) measurements as well as solar cell efficiency improvements.[19,20,23] Application results on silicon solar cells indicated more than 1% absolute efficiency gains with about 20.3% postcharging efficiency[20,23] which was identical to that of Al_2O_3 cells from the same fabrication batch.[23]

In this work, we discuss theoretical aspects such as modeling of plasma tool operation and charging mechanisms of negative and positive charge injections, based on extensive charging experiments using p-type silicon test wafers with ONO ($SiO_x/SiN_x/SiO_2$) and NO (SiN_x/SiO_2) passivation stacks. Mercury-probe C–V measurements were used to estimate the injected charge density.

This technology can be another plasma application area in addition to well-known applications for semiconductor manufacturing processes such as dry etching, thin-film deposition, sputtering, surface treatment, ion implantation, etc.[16]

II. PLASMA CHARGE INJECTION TOOL AND MODEL

The plasma charging system is schematically shown in Fig. 1(a). It consists of two functional parts: plasma generation and DC (Direct Current) biasing. Plasma is generated by a 13.56 MHz RF (Radio Frequency) power supply and confined in the upper chamber and the lower chamber is for charging a sample placed on a carrier plate to which a DC bias is applied in order to extract charges from the plasma onto the passivation dielectric surface of a wafer or a solar cell. The DC bias polarity determines the charge type to be extracted. A positive bias extracts negative charges, whereas a negative bias

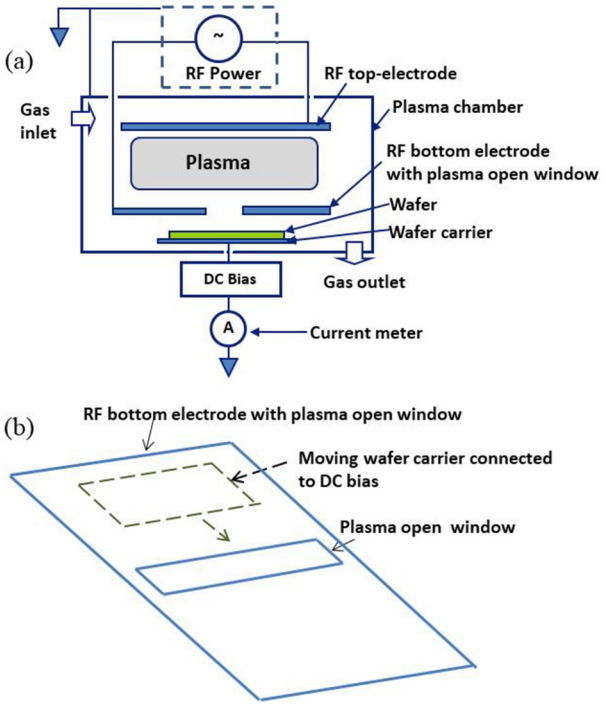

FIG. 1. (a) Schematic drawings of a plasma charging system with an RF power supply for plasma generation (a), and (b) RF bottom electrode with a plasma open window under which a wafer carrier moves from one end to the other end of a chamber, passing the plasma open window.

extracts positive charges. For this charging purpose, we use an inert gas only like helium, argon, nitrogen, etc. In an inert-gas plasma, which is a typical electropositive plasma, negative charges are electrons (but not negative ions which exist in a electronegative plasma) and positive charges are ions (ionized atoms).

Figure 1(b) schematically shows the RF bottom electrode with a plasma open area through which charges come down to a sample. The wafer carrier with a wafer (or a solar cell) held on it moves and passes under the open area for actual charging operation. Charges are introduced onto the surface passivation film when the wafer passes under the plasma opening area. Positive or negative charges can be selectively introduced depending on the bias polarity: positive charges with a negative bias or negative charges with a positive bias.

The charging current was measured by a current meter which is connected in series with the DC voltage supply, as shown in Fig. 1(a). The current is recorded every second when the wafer carrier with a DC bias applied moves from one end to the other of the chamber. Figure 2 shows a measured charging current contour as a function of time. The measured current is a DC current for a positive DC bias. The high-current plateau zone corresponds to the time when the wafer carrier passes the plasma open window in full overlap. The slope zones on both sides of the flat zone indicate the increasing and decreasing overlap area, respectively. Small currents outside the slope zones on both sides are due to straggling charges

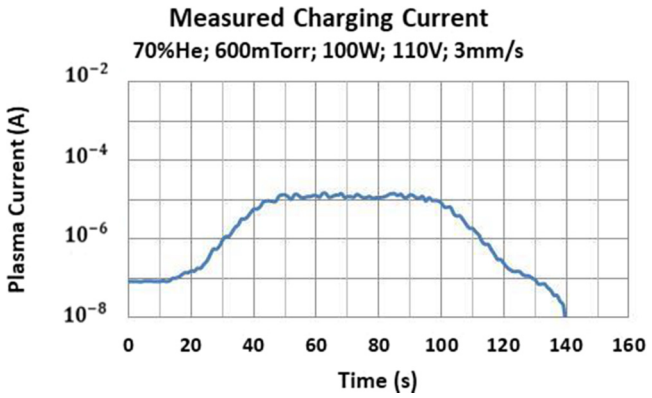

FIG. 2. Plasma charging current contour recorded while the wafer carrier travels passing under the plasma open window. The current was monitored every one second. The high current plateau time zone (45 s–100 s) corresponds to the time when the carrier passes the open window.

which are negligible for the charging purpose. The abrupt drop near 140 s is because of DC bias turn-off.

There are three key parameters on which the charging current is strongly dependent: gas type, vacuum pressure, and DC bias. For the gas type, helium is better than argon because of a less sputtering effect of passivation film as a result of its lighter atomic mass. The gas mixture with increasing N_2 fraction decreases the plasma current but makes the plasma more stable. The effects of pressure and DC bias are shown in Fig. 3 where the charging current is logarithmically plotted as a function of DC bias for three different pressures with helium gas mixed with 30% N_2. The figure indicates two important points: Firstly, the plasma charging current is approximated as an exponential function of DC bias both for positive bias and for negative bias. Secondly, for the negative bias case, the plasma current has a very weak function

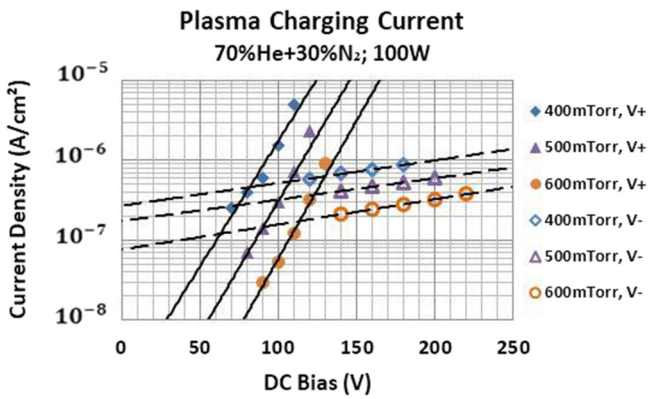

FIG. 3. Measured plasma charging currents as a function of DC bias (positive and negative) for three different pressures (400, 500, and 600 mTorr). The current is approximated to be an exponential function of DC bias for respective bias polarity.

TABLE I. Experimentally determined exponential coefficient values; A and B.

	400 mTorr	500 mTorr	600 mTorr
V+ (positive bias)			
A (A/cm^2)	1.29×10^{-9}	1.47×10^{-10}	1.92×10^{-11}
B (V^{-1})	7.21×10^{-2}	7.66×10^{-2}	8.05×10^{-2}
V− (negative bias)			
A (A/cm^2)	3.49×10^{-7}	2.71×10^{-7}	1.74×10^{-7}
B (V^{-1})	6.55×10^{-3}	6.19×10^{-3}	7.26×10^{-3}

of DC bias compared to the positive case. The difference between positive (V+) and negative bias (V−) appears to be related to the collected charge type, i.e., electron for positive bias and + ions for negative bias. The measured current values in the plot are those averaged over the plateau zone for each case similar to that in Fig. 2.

The plasma charging current density obtained from the measured current divided by the plasma window area is expressed as a function of DC bias

$$J = A \exp(B \cdot V_{dc}). \quad (1)$$

The experimentally determined values of the exponential coefficients A and B for positive and negative bias cases are summarized in Table I for three different pressures.

In an actual charging process in which charges are extracted from plasma and introduced into the surface dielectric passivation film of a cell, the current is not a fixed DC current any more but decreases as the charging goes on because of decreasing potential at the top surface of the sample. This actual charging process may be explained by the equivalent circuit shown in Fig. 4. V_{dc} is a fixed DC bias, V_{co} is a capacitor voltage due to initial fixed charges like positive fixed charges in a SiN_x film, and $V(t)$ is the potential on

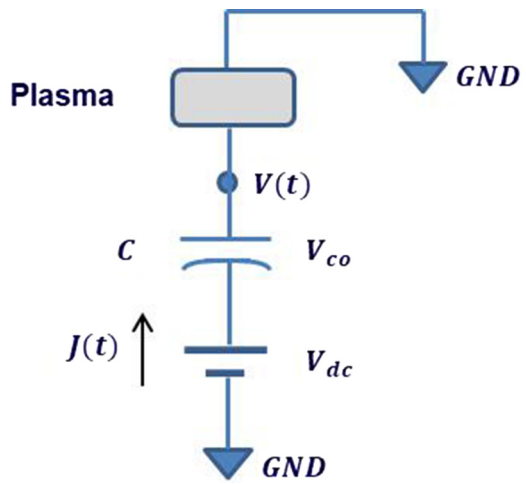

FIG. 4. Equivalent electrical circuit of a plasma charging operation.

the top surface of the passivation film of a sample cell which determines the plasma current according to Eq. (1). This exponential function allows us to obtain an analytical form for a correlation between a charging time and a flat-band voltage shift (ΔV_{fb}) or an injection charge density, for a given DC bias.

The net charge (Q) stored at the capacitance (C) by plasma charging is given as

$$Q(t) = C \cdot ((V_{dc} + V_{co}) - V(t)). \quad (2)$$

The current density is given as a derivative of charge density with respect to time as well as an exponential function of surface potential V

$$J(t) = \frac{dQ}{dt} = -C \cdot \left(\frac{dV}{dt}\right) = A \exp(B \cdot V(t)). \quad (3)$$

Equation (3) is rearranged as

$$-\frac{A}{C}\, dt = \exp(-B \cdot V(t))dV. \quad (4)$$

The left side of Eq. (4) is integrated with respect to time from 0 to t and the right side is integrated with respect to voltage from the initial potential $(V_{dc} + V_{co})$ at $t = 0$ to $V(t)$ at t. The integration result gives

$$t = \frac{C}{(A \cdot B)} [\exp(-B \cdot V(t)) - \exp(-B \cdot (V_{dc} + V_{co})]. \quad (5)$$

Equation (5) allows to determine the charging time to achieve a desired injection charge density Q and the corresponding V from Eq. (2) for a given charging condition which determines the two coefficients A and B of Eq. (1).

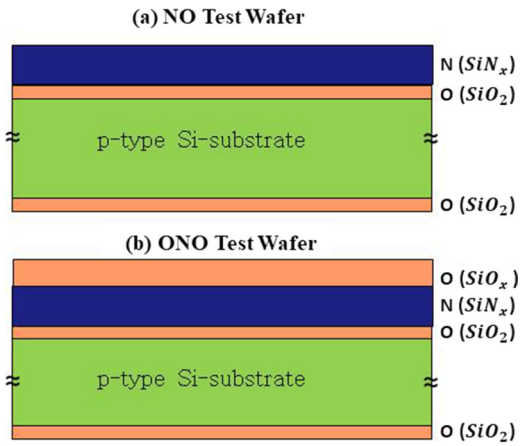

FIG. 5. Schematic drawings of a p-type silicon test wafer with a passivation stack of (a) NO and (b) ONO.

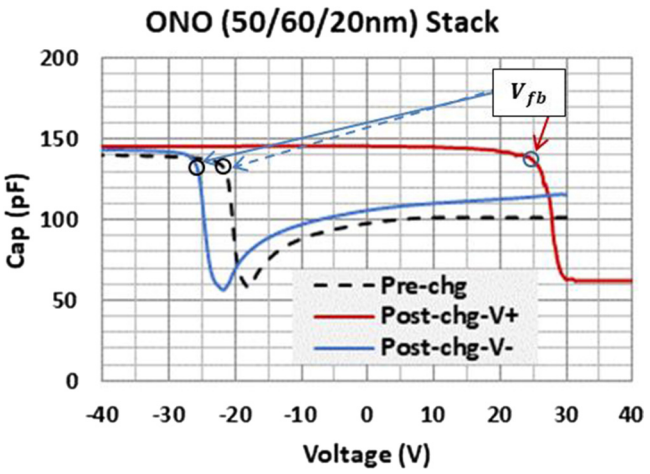

FIG. 6. C–V curves on an ONO stack sample (O/N/O = 50/60/20 nm) for three cases; precharging (dotted blue), negative charge injection (solid red), and positive charge injection (solid blue), showing significant flat-band voltage (V_{fb}) shifts in the positive direction by negative charge injection and in the negative direction by positive charge injection.

III. CHARGING EXPERIMENTS

In order to verify the charging model, we performed charging experiments using 4 in. p-type test wafers with various thickness variations of NO (nitride–oxide) stacks as well as ONO (oxide–nitride–oxide) stacks, as schematically shown in Fig. 5. The bottom oxide (SiO_2) is a thermal oxide with a thickness of about 20nm which was processed by a high-temperature thermal oxidation furnace at 855 °C in dichloroethylene (DCE) + O_2 gas ambient. The 60-nm nitride film (SiN_x) and the 50-nm top-oxide (SiO_x) were sequentially deposited with a batch-type tube PECVD tool with process conditions; temperature at 450 °C for both, pressure at 1.7 Torr for SiN_x and 0.95 Torr for SiO_x, and gas mixture with N_2O:SiH_4 = 8:1 for SiN_x and 100:1 for SiO_x.

The Mercury-probe capacitance–voltage (C–V) measurements were performed on test wafers before and after charging using a mercury probe C–V system of MDC (Material Development Corporation). All C–V measurements in this work were done with a measuring frequency of 100 kHz. The mercury-probe allows to measure C–V data by probing with mercury contacts directly on the top of a dielectric stack.

Figure 6 shows typical C–V curves on an ONO test wafer before and after charge injections. In each C–V curve, a transition point

TABLE II. Plasma charging conditions for C–V data in Figs. 7 and 8.

Gas: 70% He + 30% N_2				
	Pressure (mTorr)	RF power (W)	DC bias (V)	Time (s)
Negative charge injection	600	100	+120	1.5
Positive charge injection	350	100	−150	5

where the capacitance starts to decrease from a high constant capacitance is called flat-band voltage (V_{fb}) or voltage for no band-bending at a silicon surface. In the accumulation region (constant capacitance region in the left of V_{fb}) where the silicon surface is accumulated with majority carrier holes, the measured capacitance is the same as the insulating layer capacitance. In the depletion region on the right side of V_{fb} where the silicon surface is depleted of majority carrier holes, the measured capacitance is determined by two capacitances: the insulating layer capacitance and the silicon depletion capacitance in series. The measured capacitance rapidly decreases as the depletion region increases with increasing applied voltage. The subsequent capacitance increase for further increasing voltages is due to weak inversion layer formation at the silicon surface by minority carriers (electrons) generated by thermally and/or by light. V_{fb} is determined by two parameters: fixed charge in dielectric layers and work–function difference between silicon and top metal electrode. In this work, V_{fb} is determined mainly by the fixed charge since the work–function difference between silicon and Hg is about 0.75 eV and negligible in the voltage scale of interest.

Figure 6 illustrates how well the charging technology works. In this specific experiment, an ONO sample was used. A negative charge injection with a positive DC bias was done first and a positive charge injection with a negative bias was followed. The respective plasma charging conditions are summarized in Table II. The precharging C–V curve shows a negative flat-band voltage (V_{fb}) near −20 V which corresponds to an initial positive fixed charge density of $Q_{fix} \sim 5.3 \times 10^{12}\text{cm}^{-2}$ for the assumption of the charge location at the bottom SiN_x/SiO_2 interface. The flat-band voltage in the negative charge injection C–V curve was shifted in the positive bias direction with a flat-band voltage shift (ΔV_{fb}) of about +47 V. The following positive charge injection led to a big negative flat-band voltage shift of about −52 V.

A typical C–V curve shift by a negative charge injection for an NO stack is shown in Fig. 7. V_{fb} of the precharging C–V is about −7V corresponding to $Q_{fix} \sim 5.1 \times 10^{12}\text{cm}^{-2}$ for the charge location at the SiN_x/SiO_2 interface. It is noted that the precharging V_{fb} occurs at much lower negative bias than that of the ONO case even for the similar initial positive fixed charge density. This is because the capacitance for the NO stack is much larger than that of the ONO stack as expected from Eq. (6). A similar explanation is given to the smaller flat-band voltage shift than that of the ONO case for the same negative charge injection condition (or the similar injected charge density).

The charge density for a measured V_{fb} is obtained from the following equation:

$$Q = -C \cdot V_{fb}, \tag{6}$$

where C is a capacitance determined from the dielectric constant and the distance from the top surface to the charge location. The capacitance formula and their values for two charge location cases in ONO and NO stacks, respectively, are summarized in Table III, where C_{tox} is the top oxide capacitance and C_{nit} is the SiN_x capacitance. It is noted that the equivalent capacitance for the case of the uniform charge distribution in SiN_x is two times of C_{nit} because it is identical to the case of all the charges localized at the center of the SiN_x layer, meaning the effective thickness is half of the SiN_x thickness for the effective capacitance in the sense of flat-band shift.

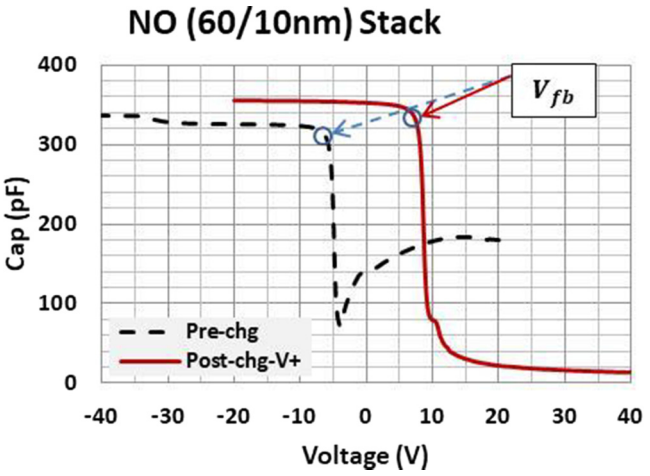

FIG. 7. Pre- and postcharging C–V curves for an NO stack, showing a much smaller V_{fb} shift than that for the ONO stack shown in Fig. 6 even for the same negative charge injection condition in Table II, which is due to a larger effective capacitance.

The injected charge densities corresponding to the flat-band voltage shifts in Figs. 6 and 7 were calculated using the capacitance values shown in Table III, and the results are summarized in Table IV.

Figure 8 shows how the potential at the top surface of the passivation stack decreases with the charge injection time. The surface potential logarithmically decreases with the charging time, as expected from Eq. (5). Figure 9 demonstrates the model verification with experimental data. We used the initial capacitance voltage (V_{co}) determined by initial positive fixed charges as a fitting parameter, because we found quite big a variation in the initial positive fixed charge density across a wafer and wafer-to-wafer even in a same batch. The V_{co} values used for fitting were −18 V, −28 V, and −40 V for $V_{dc} = 100$ V, 110 V, and 120 V curve, respectively. The injection charge density (Q_{inj}) in Fig. 9(b) is obtained by multiplying the flat-band voltage shift (ΔV_{fb}) and the capacitance (C), in a similar way as in Eq. (6).

IV. CHARGE INJECTION MECHANISMS

Figure 10 shows a schematic band-diagram of an ONO stack which is helpful to understand possible charging mechanisms for

TABLE III. Capacitances depending on charge location for ONO and NO stacks.

Charge location	ONO stack (50/60/20 nm)	NO Stack (60/10 nm)
Local at SiN_x/SiO_2 interface	$C = \frac{C_{tox} \times C_{nit}}{C_{tox} + C_{nit}}$	$C = C_{nit}$
	42.5 nF/cm^2	111 nF/cm^2
Uniform distribution in SiN_x	$C = \frac{C_{tox} \times 2C_{nit}}{C_{tox} + 2C_{nit}}$	$C = 2\ C_{nit}$
	52.6 nF/cm^2	222 nF/cm^2

TABLE IV. Calculated injection charge densities (Q_{inj}) for two charge location cases.

Passivation type	Injected charge type	Flat-band voltage shift ΔV_{fb} (V)	$Q_{inj}(\times 10^{13}\text{cm}^{-2})$	
			Local at SiN_x/SiO_2 interface	Uniform distribution in SiN_x
ONO Stack (50/60/20 nm)	Negative	47.2	−1.25	−1.55
	Positive	−51.6	1.37	1.70
NO Stack (60/10 nm)	Negative	15.0	−1.04	−2.08

negative and positive charge injections. The charge-storing SiN_x layer is sandwiched with top and bottom oxide layers and forms a potential well which confines trapped charges and minimizes the charge loss by postcharging high-temperature process. The band-diagram for the NO stack is not shown here but is easily visualized by removing the top oxide portion in Fig. 10.

A. Negative charge injection

Referring to the band-diagrams shown in Fig. 11, a most-probable charge injection mechanism is proposed as follows: Electrons extracted from plasma down to the top SiN_x or SiO_x surface of a sample are expected to have a very high energy above vacuum level in the band-diagram and to get into the top layer without seeing any energy barrier. However, high-energy electrons (hot electrons) entering into the top dielectric layer (SiN_x or SiO_x) instantaneously lose their excess energy to lattice vibration (phonon scattering), relaxing to the conduction band minimum energy.

These free electrons in the conduction band drift toward the bottom oxide interface. Some of them may be trapped at SiN_x bandgap trap centers while they are traveling through the SiN_x layer, but trapped electrons are anticipated to be reactivated to the conduction band by photons generated by plasma. Therefore, a dynamic process of electron trapping and detrapping is expected during the charging period. Some will move toward the bottom oxide interface. Once free electrons reach the bottom oxide, they are blocked by the oxide energy barrier and trapped near the interface. The distribution of injected charges is not clearly understood yet. Considering a uniform distribution of trap centers in SiN_x reported

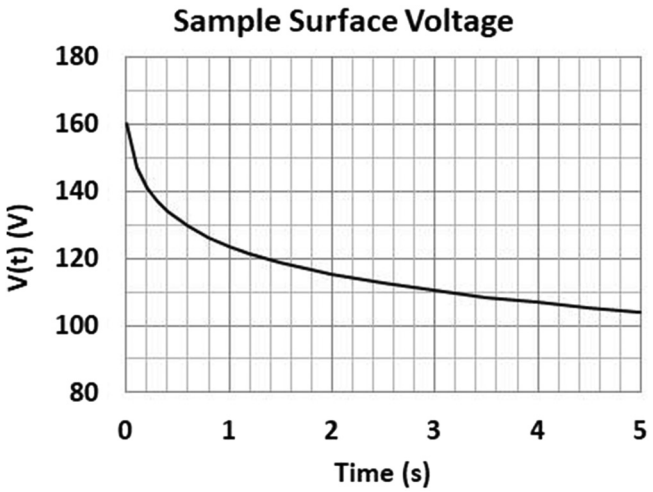

FIG. 8. Passivation film surface potential decrease with the charging time, calculated using Eq. (5) for an ONO stack, plasma operation condition (70%He + 30%N_2, 600 mT, 100 W), V_{dc} = 120 V, and V_{co} = 40 V.

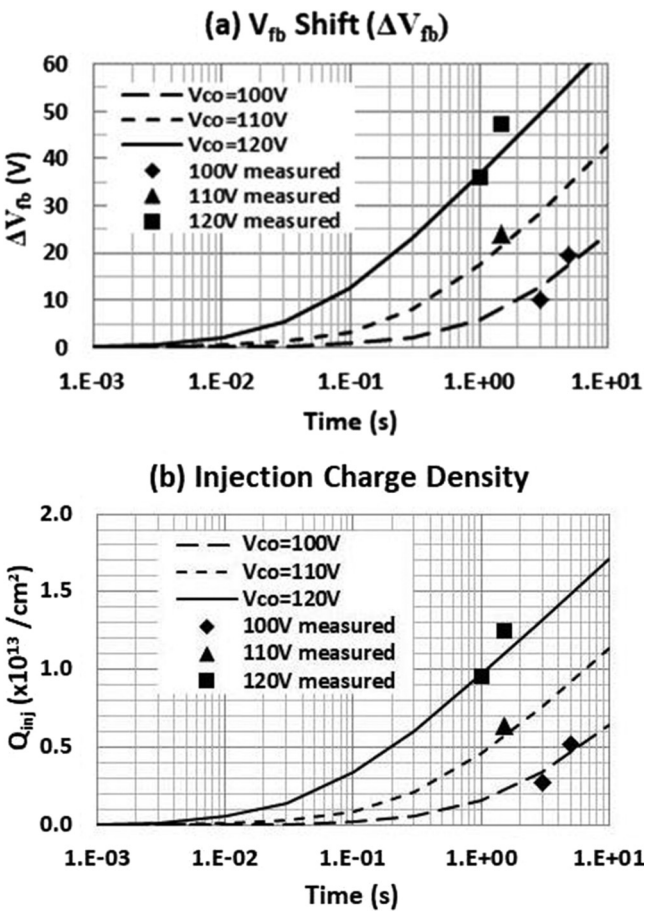

FIG. 9. Model fittings with experimental data on an ONO stack for the (a) flat-band voltage shift (ΔV_{fb}) and (b) injection charge density (assuming localized charges at the SiN_x/SiO_2 interface). Plasma operation condition: 70%He + 30%N_2, 600 mT, 100 W.

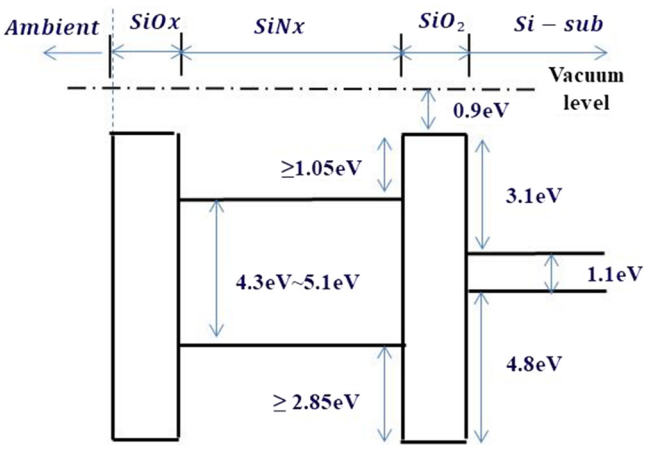

FIG. 10. Schematic band-diagram for an ONO (oxide–nitride–oxide) passivation stack. SiN_x bandgap varies depending on its composition, decreasing with increasing silicon composition for 5.1 eV for stoichiometric silicon-nitride (Si_3N_4).

earlier,[17] one may expect that the injected negative charge distribution is expected similar to the trap center distribution, which needs to be experimentally verified.

It should be pointed out that too excessive charge injection should be avoided. Charges accumulated at the bottom oxide interface build up an electric field (E-field) with a band bending in the bottom oxide. The electric field (E_{ox}) is determined by the charge amount at the interface, $E_{ox} = Q/\varepsilon_{ox}$, where ε_{ox} is the oxide dielectric constant. More charge accumulation leads to more band-bending and, thus, a higher E-field. Some injected charges may be lost to a silicon substrate via Fowler–Nordheim (F–N) tunneling[18] which is an exponential function of E-field and energy barrier (the energy height from the SiN_x conduction band minimum to the SiO_2 conduction band minimum in this case). In addition, F–N tunneling electrons become hot electrons at the SiO_2/Si interface and damage the interface, resulting in the generation of interface states.

B. Positive charge injection

The positive charge injection case with a negative DC bias is expected, which is quite different from the negative charge injection case discussed above. In the positive charge injection, positive ions are extracted from the plasma. As schematically shown in Fig. 12(a) for an NO stack, it is anticipated that accelerated positive ions hit the top surface of the passivation stack (SiN_x or SiO_x) and generate electron–hole pairs by impacting high-energy ions. Free electrons recombine with positive ions at the surface. Free holes in the valance band are trapped at bandgap trap centers in SiN_x while they move toward the bottom oxide interface, leading to more positive charges in SiN_x. It is pointed out that surface sputtering can take place if ion energy is high enough to break bonds.

For the ONO stack shown in Fig. 12(b), it is anticipated that most of the generated free holes by ion bombardments pass the top oxide due to relatively few trap centers in the top oxide and are trapped in SiN_x while they move toward the bottom oxide, which is similar to the NO stack case.

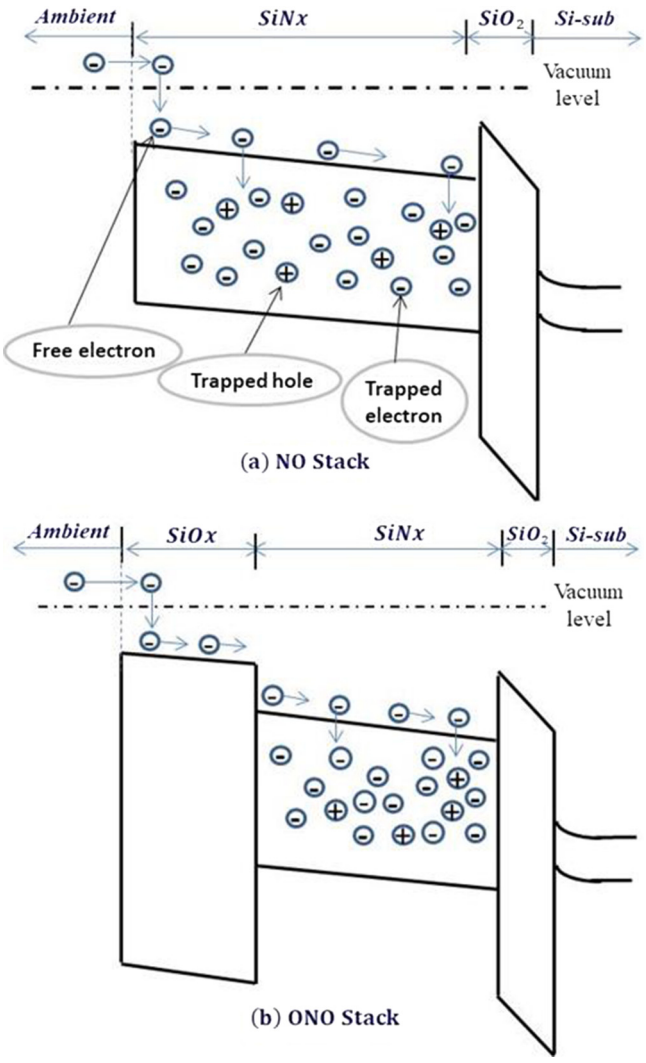

FIG. 11. Possible mechanism of negative charge (electron) injection for an (a) NO stack and (b) ONO stack. Free electrons extracted from plasma, which have an energy higher than vacuum level, easily get into the top dielectric film (SiN_x or SiO_x) and instantaneously lose their excess energy to lattice vibration, relaxing to the corresponding conduction band minimum. Some of them are trapped in SiN_x while they move toward the bottom oxide.

V. CHARGE STABILITY

The stabilities of injected charges for high-temperature metal firing and UV (ultraviolet) light illumination are of concern and need to be investigated thoroughly and improved before this charging technology is fully utilized for mass production. A previous study indicated no significant thermal stability issue for high-temperature operation with a projected lifetime over 100 years even for a 100 °C operation.[21] As far as the UV stability is concerned, there was a promising report that an optimized ONO stack gives a good stability for UV lights with a wavelength of 310 nm or longer

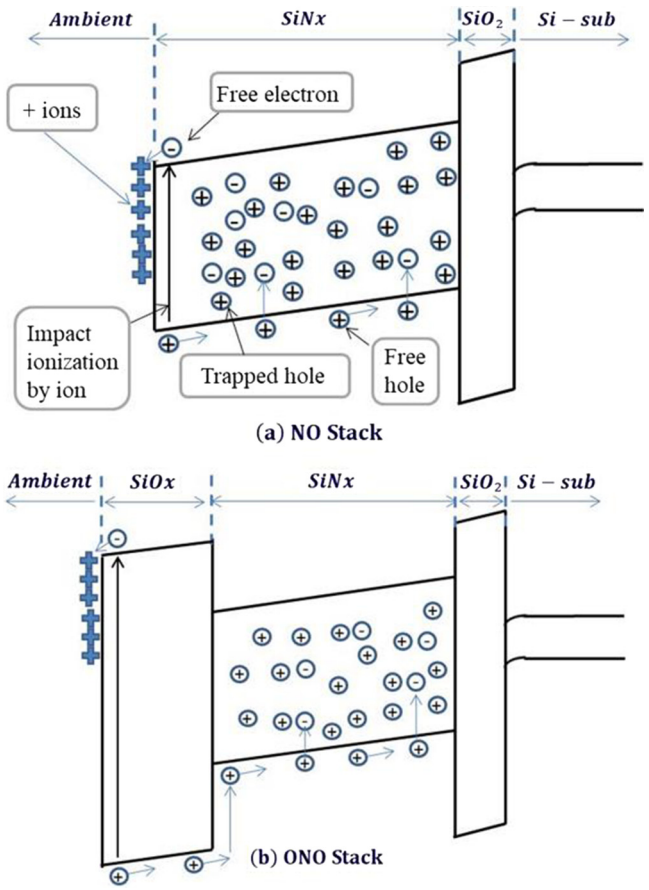

FIG. 12. Possible mechanism of positive charge (hole) injection for an (a) NO stack and (b) ONO stack. Electron-hole pairs are generated at the surface of the top dielectric film (SiN_x or SiO_x) by high-energy ion bombardment, free electrons immediately recombine with positive ions at the surface, and free holes move toward the bottom oxide and are trapped at trap centers in SiN.

(photon energy of 4 eV or lower), in addition to a good thermal stability.[22] It should be pointed out that UV lights with a wavelength of 310 nm or shorter are negligible in a terrestrial solar spectrum. Even if some exist, most of them are expected to be absorbed through module glass and the underlying EVA (ethylene vinyl acetate) encapsulant film in solar modules.

UV stability is of concern mostly to n-type cells charged on the front side. In p-PERC cells, UV stability is not a concern because the charged passivation stack is on the back which is not exposed to direct sunlight. Even in bifacial PERC whose market grows fast, the UV stability may not be an important issue because UV lights will be absorbed at reflecting objects on the ground, and, thus, reflected lights are expected to contain almost no UV component.

In mono-facial PERC cells in which the charging process is done before the metal firing process, there is the charge stability concern for a metal firing process at a high temperature above 700 °C. However, it is noted that this firing stability issue may be avoided in bifacial PERC cells because the charging process can be done on the back of finished cells.

These reliability topics have not been fully investigated yet, although some preliminary work was done earlier.[23] Thorough and extensive investigations, including optimization of stack deposition recipes, need to be made for an in-depth understanding of these topics and solve reliability-related issues.

VI. CONCLUSIONS

We have demonstrated a plasma charging technology which works well for charge injection into open field areas of a solar cell dielectric passivation stack such as NO (nitride/oxide) stack or ONO (oxide/nitride/oxide) stack in a controllable way. A charging model was proposed, and it gives a good guideline to choose a charging condition that gives a required amount of injection charges for a specific purpose. Possible charge injection mechanisms were discussed for both negative and positive charges, respectively. This plasma charge injection technique can be another application area of the well-established plasma technology. This charging technology can be a simple low-cost alternative to the complex Al_2O_3 passivation technology. However, the stability of injected charges must be demonstrated before it is fully utilized for mass production.

ACKNOWLEDGMENTS

This work was supported by the Department of Energy (Award No. DE-EE0007189). The author would like to thank the UCEP Group of Georgia Institute of Technology, particularly Eunhwan Cho and Young-Woo Ok, for processing test wafers and for processing and testing solar cells, and Dr. Ajeet Rohatgi for fruitful discussions. The author also would like to thank Paul Richter of BTU International for plasma charging runs and mercury-probe C–V measurements.

REFERENCES

[1]G. Dingemans and W. M. M. Kessels, J. Vac. Sci. Technol. A **30**, 040802 (2012).
[2]A. G. Aberle, Sol. Energy Mater. Sol. Cells **65**, 239 (2001).
[3]J. Schmidt and M. Kerr, Sol. Energy Mater. Sol. Cells **65**, 585 (2001).
[4]A. W. Blakers, A. Wang, A. M. Milne, J. Zhao, and M. A. Green, Appl. Phys. Lett. **55**, 1363 (1989).
[5]S. Dauwe, L. Middlestadt, A. Metz, and R. Hezel, Prog. Photovolt. Res. Appl. **10**, 271 (2002).
[6]G. Agostinelli, A. Delabie, P. Vitanov, Z. Alexieva, H. F. W. Dekkers, S. De Wolf, and G. Beaucarne, Sol. Energy Mater. Sol. Cells **90**, 3438 (2006).
[7]B. Hoex, S. B. S. Heil, E. Langereis, M. C. M. van de Sanden, and W. M. M. Kessels, Appl. Phys. Lett. **89**, 042112 (2006).
[8]B. Hoex, J. Schmidt, P. Pohl, M. Van de Sanden, and W. Kessels, J. Appl. Phys. **104**, 044903 (2008).
[9]J. Schmidt, A. Merkele, R. Brendel, B. Hoax, M. C. M. van de Sanden, and W. M. M. Kessels, Prog. Photovolt. Res. Appl. **16**, 461 (2008).
[10]B. Hoex, J. Schmidt, R. Bock, P. Altermatt, M. C. M. van de Sanden, and W. M. M. Kessels, Appl. Phys. Lett. **91**, 112107 (2007).
[11]M. H. White, D. A. Adams, and J. Bu, IEEE Circuits Dev. **16**, 22 (2000).
[12]J.-S. Chang, P. Lawless, and T. Yamamoto, IEEE Trans. Plasma Sci. **19**, 1152 (1991).
[13]M. Schoefthaler, R. Brendel, G. Langguth, and J. H. Werner, in *Proceedings of 1st WCPEC, Hawaii* (IEEE, New York, 1994), p. 1509.

[14]S. Glunz, D. Biro, S. Rein, and W. Warta, J. Appl. Phys. **86**, 683 (1999).
[15]K. J. Weber and H. Jin, Appl. Phys. Lett. **94**, 063509-1 (2009).
[16]N. Hershkowitz, IEEE Trans. Plasma Sci. **26**, 1610 (1998).
[17]D. T. Krick, P. M. Lenahan, and J. Kanicki, J. Appl. Phys. **64**, 3558 (1988).
[18]A. Gupta, P. Feng, M. Song, M.-L. Lin, D. Wollesen, K. Chen, and C. Hu, IEEE Electron Device Lett. **18**, 580 (1997).
[19]E. Cho, Y.-W. Ok, J. Hwang, A. D. Upadhyaya, J. K. Tate, F. Zimbardi, and A. Rohatgi, in *Proceedings of 43rd IEEE Photovoltaic Specialist Conference* (IEEE, New York, 2016), p. 2874.
[20]E. Cho, Y.-W. Ok, J. Hwang, A. D. Upadhyaya, J. K. Tate, F. Zimbardi, and A. Rohatgi, in *Proceedings of 44th IEEE Photovoltaic Specialist Conference* (IEEE, New York, 2017), p. 333.
[21]Y. Ren, K. J. Weber, and N. M. Nursam, Appl. Phys. Lett. **98**, 122909 (2011).
[22]M. Wrana, M. Schmidt, and D. Braunig, Semicond. Sci. Technol. **12**, 369 (1997).
[23]J.-M. Hwang, Final Scientific Technical Report-Amtech Systems Report No. DE-EE0007189, 2017.